UNIVERSITY OF CALIFORNIA SAN DIEGO

Probing SARS-CoV-2 Spike Protein Receptor Binding Domain Dynamics via Hydroxyl Radical Protein Footprinting

A Thesis submitted in partial satisfaction of the requirements
for the degree Master of Science

in

Chemistry

by

Kezia M. Jemison

Committee in charge:

Professor Lisa M. Jones, Chair
Professor Rommie E. Amaro
Professor Elizabeth A. Komives
Professor Brian. S. Leigh

2024

The Thesis of Kezia M. Jemison is approved, and it is acceptable in quality and form for publication on microfilm and electronically.

University of California San Diego

2024

DEDICATION

This work is dedicated to my family, my friends, and mentors, past, present, and future. I appreciate you and all your unrelenting support more than I could ever articulate. Additionally, this is dedicated to all past versions of me that doubted I could get to this point in my career and in my life. You all pushed me, whether that be out of my comfort zone or to put my best effort into everything, but you made me better myself. I thank you for it all, the good and the bad, and I promise to continue to do my best to do better for myself. I know that it will be enough to make you proud.

TABLE OF CONTENTS

LIST OF ABBREVIATIONS

FPOP	Fast Photochemical Oxidation of Proteins
hACE2	Human Angiotensin-Converting Enzyme 2
SARS-CoV-2	Severe Acute Respiratory Syndrome Coronavirus 2
RBD	Receptor Binding Doman
NTD	N-Terminal Domain
WT	Wild-Type

LIST OF FIGURES

LIST OF TABLES

ACKNOWLEDGEMENTS

I would like to acknowledge Professor Lisa M. Jones for their support as the chair of my committee, along with the rest of my committee members Professors Rommie E. Amaro, Elizabeth A. Komives, and Brian S. Leigh. Their patience and guidance have been pivotal in my development as a scientific researcher and human. I'd also like to acknowledge the outstanding work from our collaborators in the Amaro Lab that inspired this study. Additional thanks to Dr. Selina Zhi Cheng, Dr. Emily E. Chea, Scot R. Weinberger, and everyone at GenNext® Technologies for their expertise and hospitality, without which this work would not have been possible. Thank you all!

VITA

2018	Diploma, Plymouth-Whitemarsh Senior High School
2020-2022	Research Assistant, Duquesne University
2022	Bachelor of Science, Duquesne University
2022-2024	Teaching Assistant, University of California San Diego
2024	Master of Science, University of California San Diego

FIELDS OF STUDY

Major Field: Chemistry

Studies in Analytical and Computational Biochemistry & Biophysics
Professors: Lisa M. Jones and Rommie. E. Amaro

ABSTRACT OF THE THESIS

Probing SARS-CoV-2 Spike Protein Receptor Binding Domain Dynamics

via Hydroxyl Radical Protein Footprinting

by

Kezia M. Jemison

Master of Science in Chemistry

University of California San Diego, 2024

Professor Lisa M. Jones, Chair

The Severe Acute Respiratory Virus 2 (SARS-CoV-2) virus is responsible for the Coronavirus Disease 2019 (COVID-19) pandemic that continues to plague present-day society as new variants with increased virulence emerge. Viral infection may only occur once the host cell's angiotensin-converting enzyme 2 (ACE2) receptor binds to an exposed viral spike glycoprotein's Receptor Binding Domain (RBD) in its "up" state. Over the years as new variants emerged, an increase in infectivity has been observed. We hypothesize that mutations observed in later variants contribute to RBD instability, resulting in a greater likelihood of an RBD up spike. To elucidate the relationship between RBD dynamics and increased virulence amongst SARS-CoV-2 Wuhan 2019/Wild-type (WT), Delta, and Omicron variants, the MS-based protein footprinting method fast photochemical

oxidation of proteins (FPOP) was performed using GenNext® Technologies' Flash Oxidation (FOX®) system. As glycans are preferentially labeled, this instrument simultaneously allows for sufficient glycoprotein labeling via UV-based radical dosimetry and ensures user safety by generating hydroxyl radicals via lamp-based photolysis of hydrogen peroxide. Preliminary results show the FOX® system may be utilized to perform *in vitro* FPOP studies on the SARS-CoV-2 spike glycoprotein, however, further optimization is needed for more accurate comparison across conditions to discuss virulence in relation to spike structure.

Chapter 1 – Introduction

1.1 Coronaviruses and COVID-19

Coronaviruses are large, enveloped RNA viruses that cause disease within the respiratory, gastrointestinal, and nervous systems of humans and other animals.[1] Most notable examples are human coronavirus (HCoV), middle east respiratory syndrome (MERS-CoV), and severe acute respiratory syndrome (SARS-CoV). As MERS- and SARS-CoV are found in bats, coronaviruses were thought incapable of crossing species until the 2002 SARS-CoV and 2012 MERS-CoV outbreaks.[2] Most recently, there was an outbreak in 2019 of a novel coronavirus, SARS-CoV-2, in Wuhan, China that spread rapidly worldwide leading to the Coronavirus Disease 2019 (COVID-19) pandemic. Since its start, over 775 million cases were confirmed and over 7 million deaths were reported. The most recent World Health Organization update regarding COVID-19 from July 15th, 2024, details a stable number of new cases with over 150,000 between the first 28-day period to the second. Within the same timeframe, there were more than 2000 new deaths, a 3% decrease compared to the previous 28-day period. New variants emerge as SARS-CoV-2 continues to evolve to evade the immune system, thus allowing for such high positive reported COVID cases. As of March 2023, the World Health Organization's variants of concern are Alpha (B.1.1.7), Beta (B.1.351), Gamma (P.1), Delta (B.1.617.2) and Omicron (B.1.1.529). Each SARS-CoV-2 variant contains mutations that contribute to their respective infectivity and ability to evade immune response. These mutations affect the RNA that codes the whole virion, but of particular interest is the spike (S) glycoprotein.

1.2 Role of Spike Protein in SARS-CoV-2 Viral Infection

The SARS-CoV-2 spike (S) glycoprotein is a class I viral fusion protein located on the outer envelope of the virion that plays a critical role in host cell recognition and mediating fusion of the viral and cellular membranes for infection, making it a major target for neutralizing antibodies.[3] A schematic of the full-length spike protein monomer is shown in Figure 1. The heavily glycosylated homotrimer has two major subunits, S1 and S2. In the prefusion spike state, S1 contains the following four domains:

amino-terminal (N-terminal) domain (NTD), Receptor Binding Domain (RBD) and two carboxy-terminal domains (CTD1 and CTD2). The NTD contains the majority of the N-glycans, the RBD binds angiotensin-converting enzyme 2 (ACE2) of host epithelial cells at the Receptor Binding Motif (RBM) within the RBD for host cell recognition, and the CTDs contribute to the stabilization of the prefusion state. The S2 roots the protein within the membrane and contains the fusion peptide (FP) and heptad repeats (HR1 and HR2), which are necessary for viral fusion.[4]

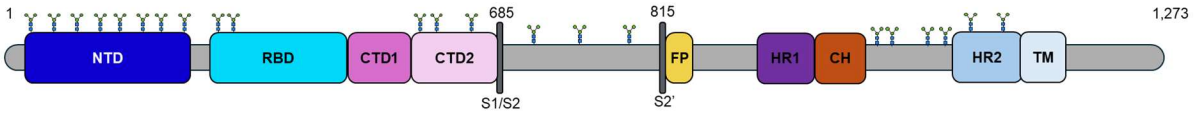

Figure 1. Schematic of the full-length SARS-CoV-2 spike protein monomer and its subdomains.

When bound to ACE2, the spike glycoprotein undergoes dramatic conformational change from a pre-fusion to a post-fusion state. This structural transition allows the protein to "puncture" the host cell membrane to trigger infection. S1 and S2 subunits are non-covalently bound in the prefusion state such that the S2 can refold to form the postfusion elongated spike that is inserted into the target cell membrane for viral entry.[4] Like SARS-CoV, the SARS-CoV-2 spike in the RBD "up" conformation is a prerequisite for ACE2 recognition and therefore infection.[5–7] Evolutionary mutations resulting in different SARS-CoV-2 alter the spike structure and properties, which contributes to differences is infectivity and virulence.

Mutations to the NTD and RBD of the SARS-CoV-2 spike have been shown to cause refolding with potential to affect viral infectivity and immune response.[8,9] The D614G mutation evolved between the Wild-Type (WT) and Alpha spike variants led to an observed increase in SARS-CoV-2 transmission making it a likely advantage for human infection as it is conserved in variants emerging today.[10,11] This point mutation results in the loss of a stabilizing disulfide bridge with residue K854 at the base of the RBD (Figure 2), allowing for increased RBD range of motion and therefore a greater likelihood of the RBD "up" state capable of recognizing ACE2 for infection. Additionally, glycans were shown to play significant roles in the RBD opening process. Glycans at positions N165 and N234 actively supports the

RBD in the "up" conformation while N343 pushes the RBD upward.[12,13] As a homotrimer, the spike can exist in either the 1- or 2-RBD up intermediate states before proceeding to the full open spike conformation. Further, the spike protein RBDs may have varying degrees of openness as the spike transitions from closed to open such that host cell recognition would not occur as the RBD would not be "up" enough for ACE2 to bind.

Improving our understanding of SARS-CoV-2 viral entry will allow for the development of treatment and prevention methods of diseases with similar mechanisms. This work aims to help elucidate why SARS-CoV-2 is so infectious by using protein footprinting to assess RBD opening dynamics of the Wuhan-2019/Wild-Type (WT), Delta (Δ), and Omicron (O) spike proteins. As RBD openness increases, the likelihood of infection increases as a 1-up RBD state is required for host cell recognition and the RBD must be "up" or open enough for ACE2 to bind. Solvent accessibly would also increase as the RBD opens, exposing previously obscured residues. Using the protein footprinting method Fast Photochemical Oxidation of Proteins (FPOP) coupled to Mass Spectrometry would allow for the identification of exposed RBD and spike sites via oxidative modification and downstream quantification. Differential analysis will be performed between closed and open spike states to compare the degree of RBD openness across WT, Delta, and Omicron spike variants.

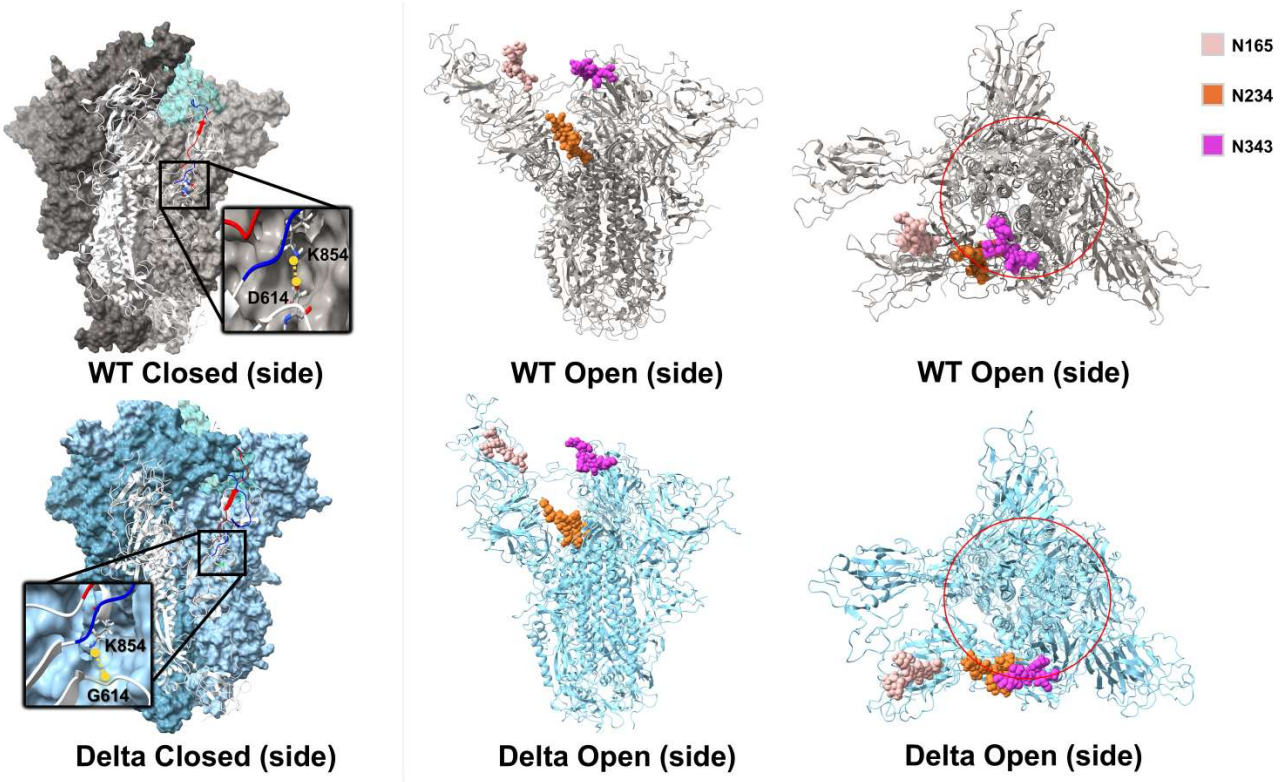

Figure 2. Amaro Lab MD predictions of WT and Delta RBD open/1-up vs closed/locked-down spike states suggest a higher degree of RBD opening for Delta and Omicron variants due to the evolved D614G mutation resulting in the loss of stabilizing D614-K854salt bridge. Consequently, glycans N165, N234, and N343 have different distances in relation to one another and the center of the trimer.

1.3 Summary of Introduction

SARS-CoV-2 is the pathogen responsible for COVID-19. Viral infection is triggered when SARS-CoV-2 spike glycoprotein in RBD "up" state binds to ACE2 and the spike transitions from a prefusion to post-fusion conformational, "puncturing" the host cell membrane providing means of viral entry for replication. The heavy glycosylation of the spike protein protects the virus from the immune system defense response by providing a "sugary shield". In addition to shielding, three of the spike's glycans (N165, N234, N343) play active roles in RBD opening.[12] Varying degrees of spike RBD opening are predicted with later variants hypothesized to be more open due to the RBD destabilizing D614G mutation, suggesting emerging variants are more likely to be in an RBD "up" state and thus more likely to trigger the infection cascade. In this thesis, an in vitro FPOP study is presented to investigate the hypothesized increased degree of RBD dynamics in emerging variants of the SARS-CoV-2 spike glycoprotein.

Chapter 2 – Probing SARS-CoV-2 Spike RBD Dynamics via FPOP

2.1 An Introduction to Protein Footprinting via FPOP

Protein footprinting is a powerful technique for structural biology and biophysics and even more so when they are MS-based. Well established MS-based protein footprinting methods for dynamics and interface characterization of biomolecules and their interactions are Hydrogen Deuterium Exchange (HDX) and Hydroxyl Radical Protein Footprinting (HRPF). HDX occurs on the second timescale allowing for insights into dynamics and structure over time at peptide level resolution.[14] HRPF uses hydroxyl radicals to covalently label solvent accessible amino acids non-specifically. Overoxidation leads to unfolding, so it is imperative to optimize the concentration of hydroxyl radicals available for labeling a given protein. Hydroxyl radicals are generated in various ways. The first to note was via Fenton chemistry to study DNA.[15] Other well established methods of hydroxyl radical generation include synchrotron radiolysis[16] and laser photolyisis of hydrogen peroxide.[17,18] This method of HRPF in which proteins are labeled with hydroxyl radical generated via laser photolysis is known as Fast Photochemical Oxidation of

Proteins (FPOP). Unlike HDX, FPOP labeling occurs on the microsecond timescale, which is faster than unfolding can occur thus allowing for study of native protein structure. Since its initial development using pure proteins *in vitro*, FPOP has been extended to study the native state of proteins *in-cell*[19,20] and *in vivo*.[21]

FPOP is a useful protein footprinting method that becomes a powerful quantitative biophysical tool when coupled with Liquid Chromatography-Tandem Mass Spectrometry (LC-MS/MS). MS data is used to identify and quantify oxidation and perform differential analyses capable of providing information on conformational change and protein-protein and protein-ligand interactions at the peptide- and residue-level. FPOP uses highly reactive hydroxyl radicals to investigate protein solvent accessibility as more oxidation would be observed in more accessible regions. Theoretically, 19 out of the 20 amino acids can react with hydroxyl radicals, each with their own reactivity rate (k_{OH}) at neutral pH and possible modification detectable via downstream MS as mass change (Table 1).[22] The most reactive residues contain sulfur, like cysteine, while glycine is the least reactive, inhibiting detection of labels corresponding to mass change. Laser-based *in vitro* FPOP has been optimized to label while preserving protein structural integrity. However, the experiments herein use a semi-automatic benchtop flash oxidation system from GenNext® Technologies.

Table 1. FPOP reactivity rates and possible modifications per amino acid

Amino Acid	k_{OH} ($M^{-1} s^{-1}$)	Modification & Mass Change (Da)
Cys (C)	3.50×10^{10}	Sulfonic acid (+48), sulfinic acid (+32), hydroxy- (-16)
Trp (W)	1.30×10^{10}	hydroxy- (+16, +32, +48), pyrrol ring-open (+32)
Tyr (Y)	1.30×10^{10}	hydroxy- (+16, +32)
Met (M)	8.50×10^{9}	sulfoxide (+16), sulfone (+32), aldehyde (−32)
Phe (F)	6.90×10^{9}	hydroxy- (+16, +32)
His (H)	4.80×10^{9}	oxo- (+16), ring-open (−22, −10, +5)
Arg (R)	3.50×10^{9}	hydroxy- (+16), carbonyl (+14), deguanidination (-43)
Ile (I)	1.80×10^{9}	hydroxy- (+16), carbonyl (+14)
Leu (L)	1.70×10^{9}	hydroxy- (+16), carbonyl (+14)
Val (V)	8.50×10^{8}	hydroxy- (+16), carbonyl (+14)
Pro (P)	6.50×10^{8}	hydroxy- (+16), carbonyl (+14)
Gln (Q)	5.40×10^{8}	hydroxy- (+16), carbonyl (+14)
Thr (T)	5.10×10^{8}	hydroxy- (+16), carbonyl (−2- or +16-H_2O)
Lys (K)	3.50×10^{8}	hydroxy- (+16), carbonyl (+14)
Ser (S)	3.20×10^{8}	hydroxy- (+16), carbonyl (−2- or +16-H_2O)
Glu (E)	2.30×10^{8}	hydroxy- (+16), carbonyl (+14), decarboxylation (-30)
Ala (A)	7.70×10^{7}	hydroxy- (+16)
Asp (D)	7.50×10^{7}	hydroxy- (+16), decarboxylation (-30)
Asn (N)	4.90×10^{7}	hydroxy- (+16)
Gly (G)	1.70×10^{7}	

2.2 Methods

Here the methodology used to obtain the preliminary data reported is detailed as FPOP experiments must be optimized prior to ensure efficient and reproducible labeling glycoproteins given the preferential labeling of glycans.

2.2.1 Benchtop Flash Oxidation (FOX®) System

GenNext® Technologies' FOX® system provides a UV lamp-based alternative to hazardous and costly laser-based *in vitro* FPOP methods, making FPOP a more accessible tool.[17,18,23] Further, simultaneous measurement of effective radical dose via real-time inline UV-based dosimetry is possible.[24] An extrinsic or intrinsic dosimeter absorbs at 265 nm and either increases or decreases in absorbance, respectively, with increasing oxidation due to increasing hydroxyl radical concentration. Real-time measurement of dosimeter absorbance allows for determining the effective radical dose to better ensure efficient labeling through generation of a dose response curve. Protein buffer contents may scavenge radicals, thus performing a buffer exchange may be necessary to ensure sufficient labeling before experimentation. A dose response curve with non-linear changes in oxidation suggests artifactual

structural change due to overoxidation. Background oxidation is accounted for by applying no voltage (0 V) to sample at flash cell as a control and measuring dosimeter absorbance in the theoretical absence of hydroxyl radicals. Sample collection is semi-automatic as the workflow is automated after the injection of the 20 µL sample and the flash sequence is triggered. Eight µL of sample goes to waste and 12 µL flows to the flash cell for irradiation followed by the dosimetry cell. Here, the real-time dosimeter absorbance at 265 nm is measured before the labeling reaction is quenched with 35 mM Methionine and 100 mM DMTU and sample is collected. Figure 3 shows all modules of the FOX®.

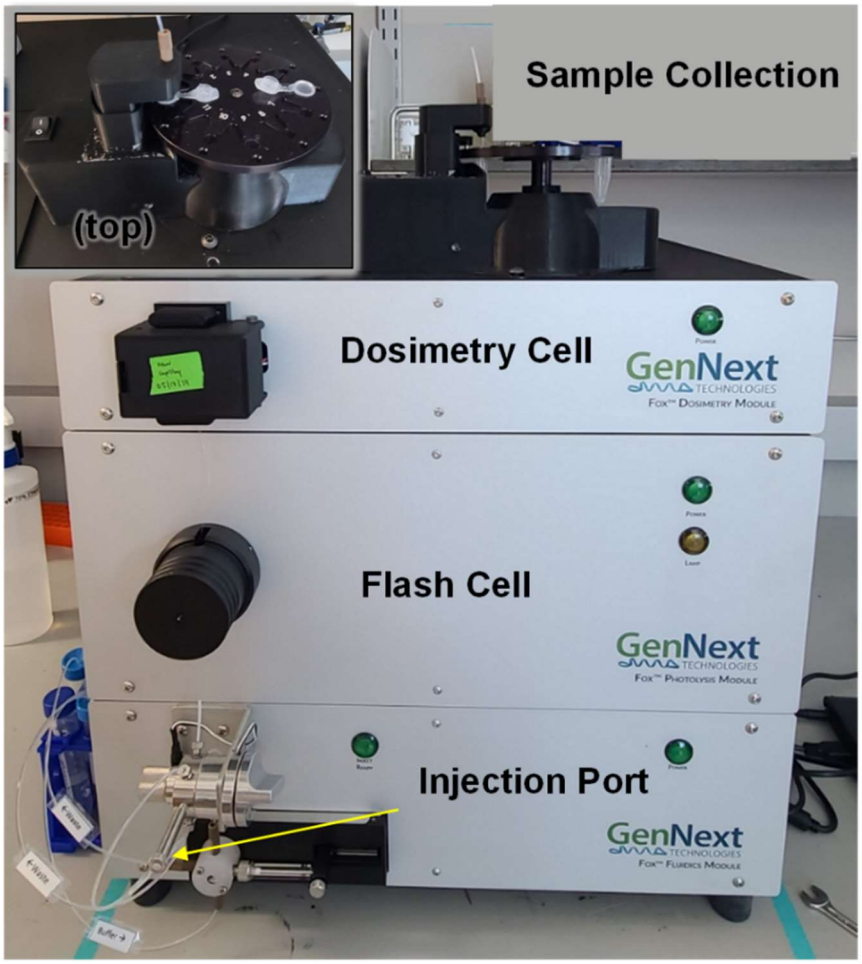

Figure 3. GenNext® Technologies' semi-automatic FOX® system. Sample is injected at the fluidics module, irradiated at the photolysis module, and collected after dosimeter absorbance is measured at the dosimetry module.

The capillary that sample flows through is Polymicro Technologies Molex clear silica tubing (1068160105) with an outer (OD) and inner diameter (ID) of 360 µm and 250 µm, respectively. For the default 12 µL sample loop, a flowrate of 15 µL/min and flash frequency of 2 Hz (or 180 maximum flashes in 60 s). These values are user specified such that need for a different flowrate and flash frequency due to changing sample loop volume could be met. The applied voltage may also be user specified (up to 1500 V), so hydroxyl radical concentration may be altered by varying the applied voltage and/or concentration of hydrogen peroxide spiked into the sample.

Here, we test the FOX® system for in vitro FPOP of the SARS-CoV-2 spike glycoprotein homotrimer to assess Receptor Binding Domain (RBD) opening/closing dynamics across Wuhan-2019/Wild-type (WT), Delta (Δ), and Omicron (O) spike variants. As glycans are preferentially labeled, this instrument simultaneously ensures sufficient labeling of the glycoprotein via UV-based in-line radical dosimetry and user safety by generating hydroxyl radicals via voltage-based photolysis of hydrogen peroxide.

2.2.2 *In vitro* FPOP Sample Preparation

PBS buffer was made by dissolving Phosphate Buffered Saline, pH 7.4 packet (Sigma P-5368) in deionized water. The following reagents were purchased from Fisher Chemical: L-methionine, 1,3-Dimethylthiourea (DMTU), dithiothreitol (DTT), hydrogen peroxide, tris base, calcium chloride, hydrogen chloride , 0.1% FA in water, and 0.1% FA in ACN. Pierce Trypsin Protease MS-Grade 5 x 20 µg (90057) was purchased from Fisher Scientific. Adenine was purchased from Sigma-Aldrich. Peptide N-Glycosidase (PNGase) F kit was purchased from New England Biolabs (P0704).

Purified proteins were purchased from SinoBiological. Open/Up conformations of the WT (40589-V08H4), Delta (40589-V08H10), and Omicron (40589-V08H26) variants of spike were purchased from the catalog. Closed/Locked-Down conformations of all variants were custom expressed and purified by introducing G413C and V987C mutations within each variant's protein sequence. WT and

Delta open spikes underwent buffer exchange to PBS using Microcon-30 Centrifugal Filter Unit (MRCF030) and following the unit's corresponding protocol. Sample was prepared with final concentrations of 1 mM Adenine and 0.18 mg/mL protein before spiking in hydrogen peroxide for 20 µL total sample volume directly before sample injection. Given the limited sample available of WT up and Delta after buffer exchange, their corresponding initial protein concentrations were less than 0.18 mg/mL (Table 2). Although initial protein concentration should be consistent to across conditions to normalize the number of accessible sites available, hydrogen peroxide concentration and/or voltage applied could differ across conditions so long as the change in absorbance between the control (zero voltage with/without hydrogen peroxide) and experimental (applied voltage with hydrogen peroxide) was ~40.00 mAU across conditions (Table 2). In other words, the effective radical dose would be consistent regardless of hydroxyl radical concentration available across conditions allowing for more accurate comparison. At least triplicates were performed for all conditions except Delta Up due to limited sample availability.

Table 2. Initial protein and H_2O_2 concentrations and voltage used to FPOP each sample and their corresponding changes in absorbance at 265 nm

Condition	Init. [Prot.] (µg/µL)	Init.[H_2O_2] (mM)	Applied Volt. (V)	$\Delta Abs_{265\,nm}$ (mAU)
W-UP	0.13	21.7	0, 900	7.56
Δ-UP	0.015	0.833	0, 900	26.77
Ω-UP	0.18	10	0, 1100	40.86
W-LD	0.18	35	0, 900	41.18
Δ-LD	0.18	10	0, 1400	45.60
Ω-LD	0.18	10	0, 1400	48.49

Once injected using a 25 µL Hamilton syringe (80465), 12 µL of the sample flowed to the flash cell at flow rate of 15 µL/min while the remainder went to waste. The sample was irradiated by the 265 nm UV lamp at a rate of 180 maximum flashes in 60 seconds and frequency of 2 Hz in the flash cell. The dosimeter absorbance was measured before the labeling reaction was quenched using a solution containing 100 mM DMTU and 35 mM Methionine. To reduce and denature, samples were incubated at 95 °C for 25 minutes with mixing at a final concentration of 50 mM Tris-HCl/1mM $CaCl_2$ and 5mM DTT. A 1:20 trypsin to protein ratio was used to digest the spike proteins overnight at 37 °C with mixing. Digestion was terminated by a 10-minute incubation at 95 °C and samples were cooled to RT before a 4-hour incubation at 37 °C with 1 µL PNGase F to deglycosylate. After deglycosylation, samples were centrifuged for 3 minutes to spin down and transferred to MS vials. Samples were acidified to a final concentration of 0.1% FA prior to MS analysis. Figure 4 describes the workflow using the FOX starting at sample preparation up to data analysis and FPOP quantitation.

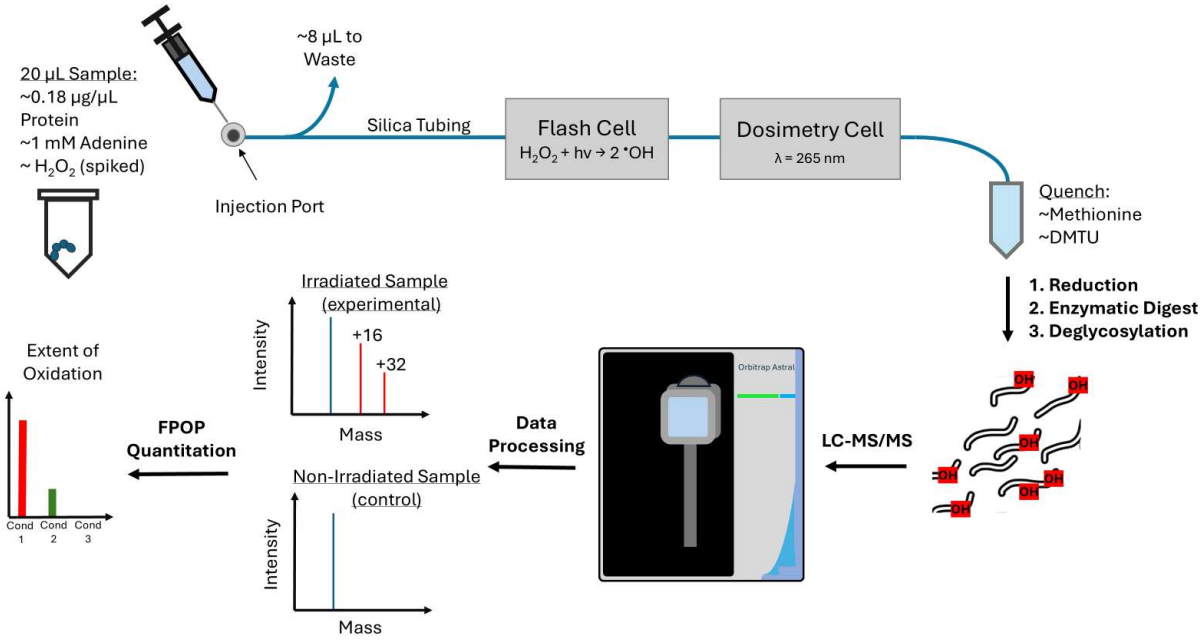

Figure 4. *in vitro* FPOP workflow using the FOX®. Protein samples containing a dosimeter (1mM Adenine) were spike with H_2O_2 before injection into the system. Once injected, 8µL went to waste while 12µL continued to flow to the flash cell to be irradiated by a 265 nm UV lamp. Subsequently, irradiated sample flows to the dosimetry cell where the dosimeter absorbance was measured in real-time. The labeling reaction was quenched when the sample reached the quench solution containing methionine and DMTU and collected in the automated sample collector for subsequent LC-MS/MS sample preparation and analysis.

2.2.3 Liquid Chromatography-Tandem Mass Spectrometry (LC-MS/MS)

As no alkylation occurred during MS sample preparation, increasing the likelihood of refolding, 2 µL 500 mM DTT was added to each digest sample prior to MS analysis to prevent refolding. Following the Evosep sample loading protocol, protein digests were loaded onto C18 Evotips. The dry C18 resin of the tips was washed with 20 µL Solvent B, centrifuged for 60 seconds at 700 x g, and conditioned by soaking in 100 µL 1-propanol until pale white. Soaked tips went through two cycles of centrifugation with 20 µL of Solvent A at 700 x g for 60 seconds to equilibrate. 300 ng of sample digest was loaded onto the wet C18 resin of the Evotip, then washed by adding 20 µL Solvent A and centrifuging for 60 seconds at 700 x g. 100 µL of Solvent A was added to tips and centrifuged at 700 x g for 10 seconds to ensure the C18 resin remained wet.

Peptides were separated using Evosep's 44-minute gradient and analyzed on an ThermoFisher's Orbitrap Astral MS. The following acquisition parameters were used: data dependent acquisition mode, scan range of 375-1200 m/z, resolution of 120000, applied intensity threshold of $5.0x10^3$, charge state range of 2-6, profile data type, positive polarity and with Field Asymmetric Ion Mobility Spectrometry (FAIMS). HCD collision energy of 30% was used to fragment peptides along with a customized AGC target of 50% normalized AGC target, auto maximum injection time, and 1 microscan.

2.2.4 Data Analysis

Raw data file outputs were converted to mzML using MSConvert[25] version (3.0.24089-fc08ea4) with peakPicking and zeroSamples filters applied. MS data was analyzed using Fragpipe (v21.1), MSFragger (v4.0), IonQuant (v1.10.12), and Philosopher (v5.1.0). Searches were performed as described previously with variable modifications (varmods) or mass offsets specified as FPOP modifications.[26] Further data processing was performed using the Excel PowerPivot add-in to quantify the extent of modification for each peptide by dividing the sum of the area of modified peptide by the sum of the area of unmodified and modified peptides.[27]

2.3 Results and Discussion

2.3.1 Results

In-line dosimetry absorbance data was used to generate dose response curves by plotting the applied voltage vs the change in absorbance of 1mM Adenine. As adenine was used as the extrinsic dosimeter, its absorbance decreased with increasing oxidation as hydroxyl radical concentration increased, resulting in a greater change in absorbance from the no applied voltage (0V) control. Dose response curves for all except Omicron open spike could not be made due to limited sample availability inhibiting more than two voltages to be tested in triplicate. As expected, linearity was observed when increasing voltage was used for labeling the Omicron spike in its open state (Figure 5).

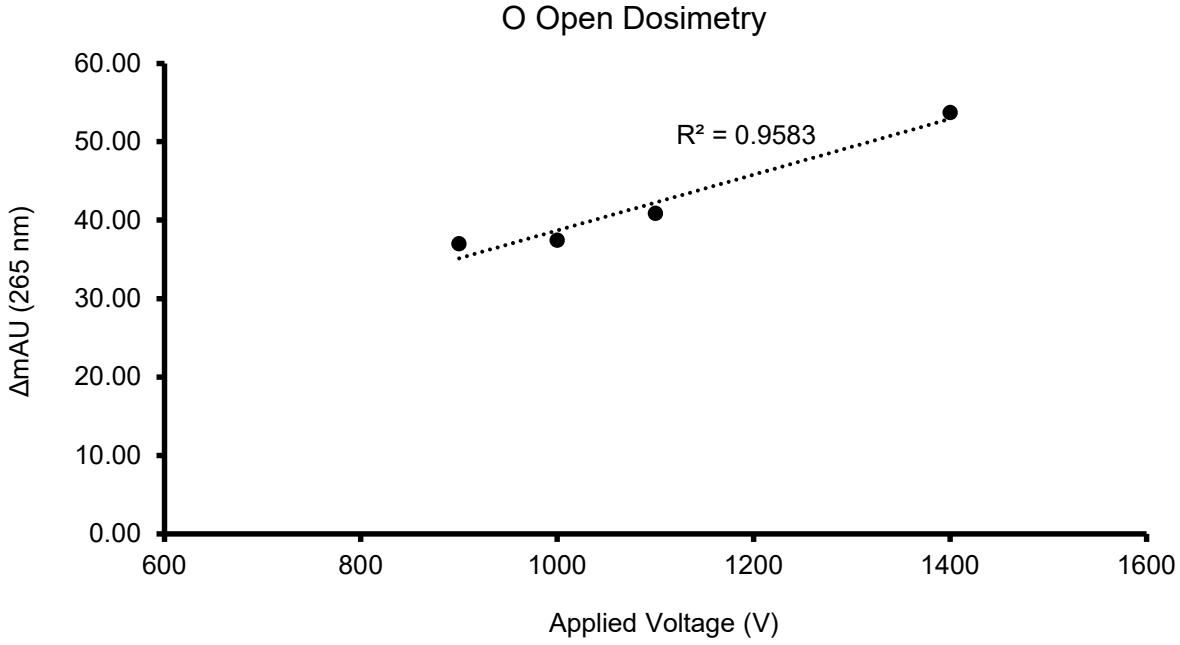

Figure 5. Omicron (O) Open spike protein dose response curve generated to assess effective radical dose based on 1 mM adenine absorbance at 265 nm.

Figure 6 shows generalized labeling coverage across all conditions on a representative spike structure based on the WT. The condition observed with the greatest number of oxidatively modified peptides out of the 11 peptides detected across conditions was the WT open spike with 9 modified peptides. Out of those 11 peptides, peptides 559-567 and 826-835 were the only two quantifiable peptides across all conditions that could be used for differential analysis. Peptide 559-567 is located closer to the

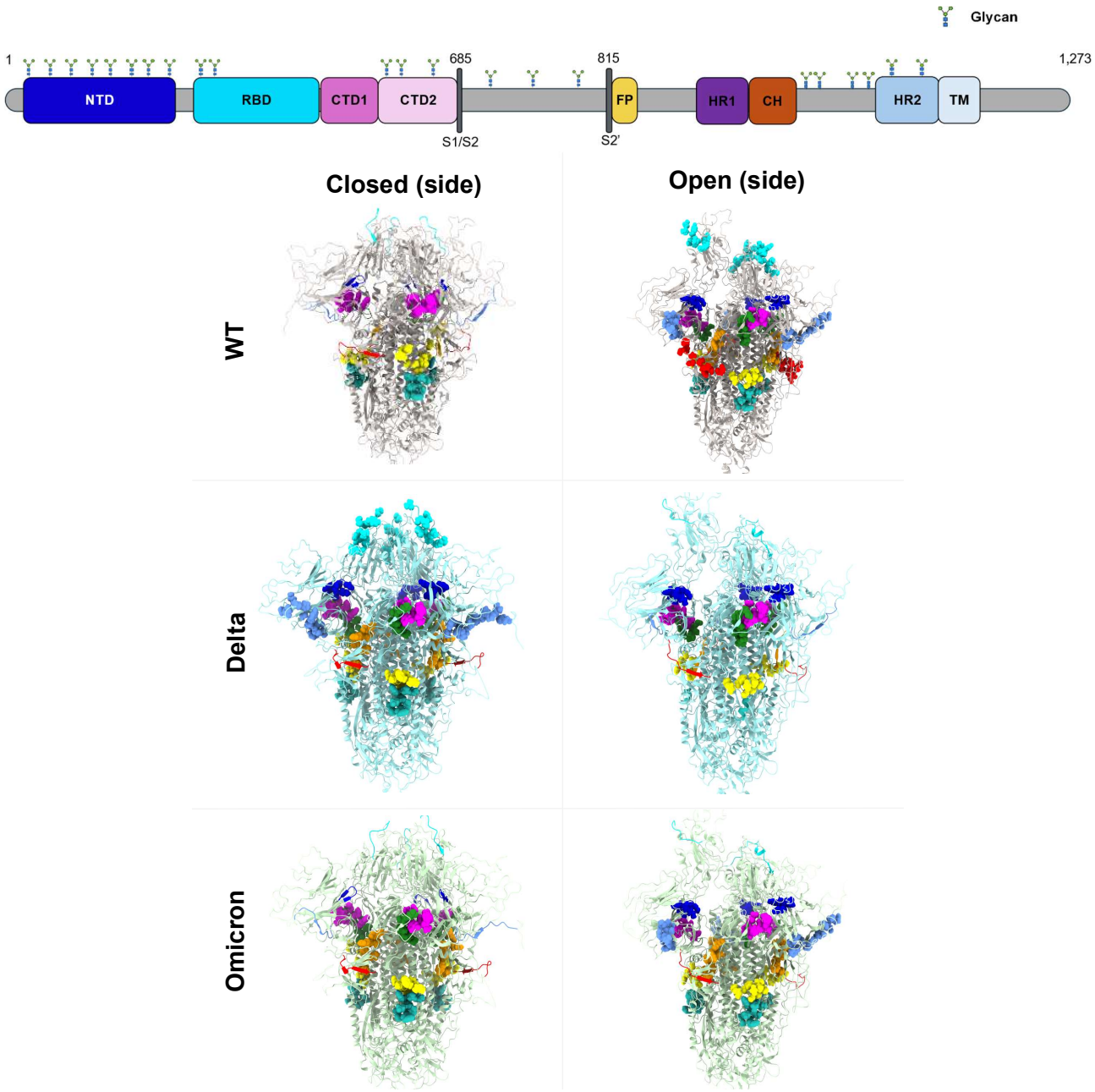

Figure 6. Labeling coverage across all spike protein conditions. Labeled peptides are represented by bubbles. Peptides detected within the NTD and RBD are represented by navy blue and teal, respectively.

RBD than peptide 826-835. Figure 7 illustrates the exposure of residues near the RBD as the RBD opens on the WT spike. Greater oxidation was observed at peptide 559-567 for WT in its open state compared to the closed state, suggesting increased solvent accessibility of peptides near RBD due to RBD opening (Figure 8). Furthermore, there was no statistically significant difference in 826-835 labeling across spike conditions, supporting the expected little to no change in solvent accessibility of peptides far away from the RBD due to RBD opening.

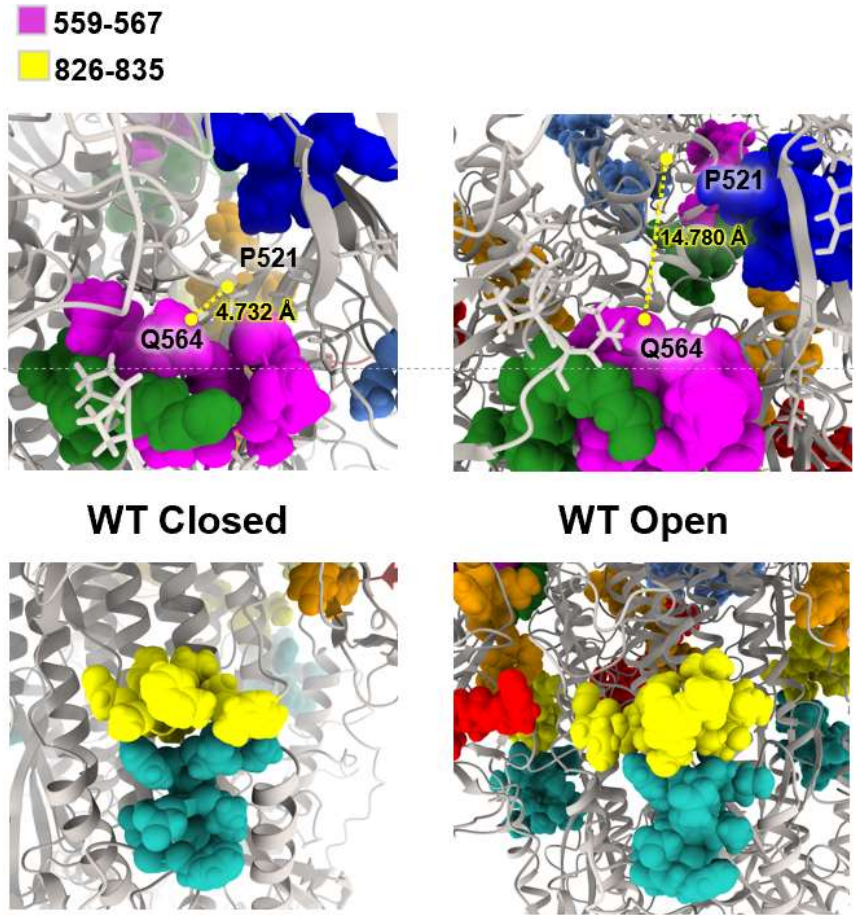

Figure 7. RBD opening of the Wild-Type (WT) increased the distance between P521 and Q564, a residue within peptide 559-567 near the RBD, suggesting increased exposure of residues close to RBD to hydroxyl radicals. Peptide 826-835 residues are unaffected by RBD opening.

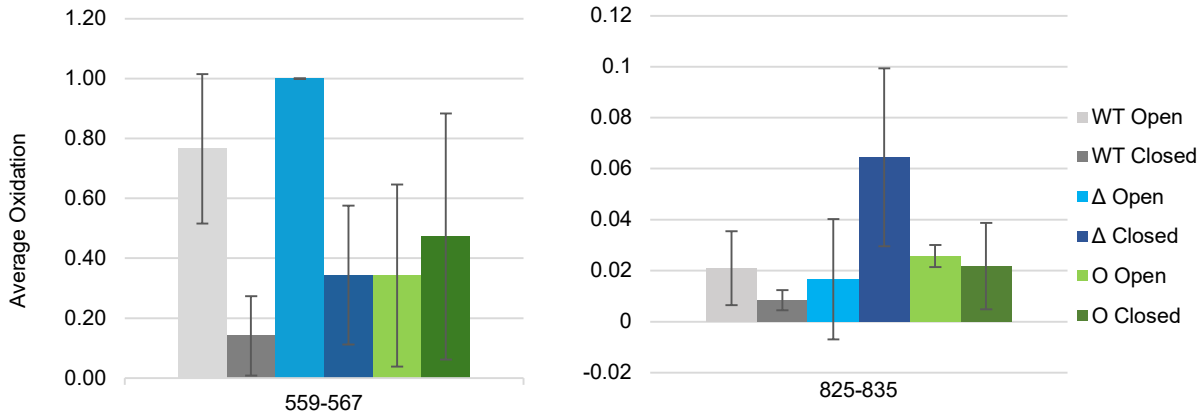

Figure 8. Average oxidation of peptides 559-567 and 826-835 across all spike conditions: Wild-Type (WT), Delta (Δ), and Omicron (O) in open vs closed states.

2.3.2 Discussion

Here, the FOX was successfully used for *in vitro* FPOP of the open/up and closed/locked-down RBD states of the WT, Delta, and Omicron SARS-CoV-2 spike proteins. Although many peptides were detected in individual spike conditions, there were only two peptides (559-567 and 826-835) with FPOP modifications that were quantifiable across each condition such that differential analysis could be performed to assess the RBD opening dynamics. More variation was introduced due to inconsistent initial protein concentrations and different number of technical replicates that possibly resulted in the inability to achieve the desired change in absorbance of ~40.00 mAU across conditions, and thus inconsistent effective radical doses were used. Although the corresponding change in absorbance is only 7.56 mAU, these results show there was a statistically significant difference between oxidation observed for the open vs closed WT spike when the open WT was delivered a lower effective radical dose. Due to the error associated with unoptimized MS sample prep workflow, Delta and Omicron data was unreliable and could not be commented on with respect to peptide level analysis at the time. Further optimization is required for MS analysis and normalized effective radical dose across spike conditions due to preferential labeling of glycans to ensure sufficient labeling of native spike protein structure such that more quantifiable peptides may be detected in all spike conditions and a more comprehensive understanding of spike RBD dynamics may be obtained.

Chapter 3 – Conclusions and Future Directions

Here we demonstrated the FOX® system can be used to perform *in vitro* FPOP to label the SARS-CoV-2 spike glycoprotein such that quantification of the resultant processed LC-MS/MS data supported the conformational difference between open vs. closed spike states. Although effective radical dose varied, label quantification showed a significant increase in oxidation on a peptide close to the RBD between open and closed spike states of the WT.Further optimization is currently underway to allow for the comparison of RBD dynamics between WT, Delta, and Omicron spike variants to further comment on the increased virulence observed of emerging SARS-CoV-2 variants. Once completed, the current *in vitro* work studying spike RBD dynamics will be extended to investigate how the SARS-CoV-2 virion travels through a dense mucin barrier prior to reaching the air/lung interface to bind ACE2 and trigger infection.

Before it can bind ACE2 at the air/lung interface, the SARS-CoV-2 virion must pass through a dense barrier MUC5AC and MUC5B respiratory mucins. These mucins are heavily *O*-glycosylated and work to expel exogenous pathogens.[28] As mucins are negatively charged and the SARS-CoV-2 spike protein evolved to be more electrostatically positive from WT to Omicron,[29] it is likely that spike-mucin binding is favorable upon host cell entry. Novel Amaro Lab simulations of MUC5AC and MUC5B bound to SARS-CoV-2 spike proteins suggest spike-mucin binding is avidity-driven and binding sites are concentrated around the RBD, NTD, and FCS of the spike. Results from locating and characterizing the spike-mucin binding “hotspots” strength and duration across spike variants in “lung-like” conditions will be compared to these novel simulations to assess the hypothesis that electrostatics drive spike-mucin binding. We hypothesize that the spike evolved to increase contacts and/or binding strength with the MUC5AC and MUC5B mucins such that later spike variants increased access to the bind ACE2, thus contributing to the observed increased infectivity of emerging variants.

The SARS-CoV-2 virus is an airborne pathogen capable of traveling up to two meters via small respiratory aerosol to infect a host. These aerosols are less than 5 μm in diameter and contain the virion in addition to mucins, albumin, and lipids.[30] During the journey from the infected individual to the new host's lung, the respiratory aerosol undergoes chemical changes capable of reducing viral viability.[31] For example, rapid dehydration would result in higher ion concentrations. Furthermore, protein may denature when exposed to an air-water interface.[32] Results obtained from using *in-vitro* FPOP-MS to characterize spike-mucin binding modes in "aerosol-like" conditions will be compared to novel Amaro lab simulations that suggest the mucins and divalent cations create a network of interactions with the spike protein, creating a protective "cage" around the virions such that the virus is able to survive the harsh aerosol conditions. We hypothesize that more binding interactions will be observed with later spike variants, allowing for increased protection and viability.

FPOP allows for mapping native protein structure such that information on conformational change, protein-ligand, and protein-protein interactions can be obtained.[17] Additional use of Hydrogen-Deuterium Exchange (HDX) would allow for additional insights on protein dynamics and structure over time given their second vs microsecond timescale difference.[14] In collaboration with the Komives Lab at UCSD, the experimental data obtained from FPOP- and HDX-MS experiments will be used to refine existing Amaro Lab computational predictions of the mucin-bound and -unbound spikes and the entire SARS-CoV-2 virion. Such studies would aid the discovery of antiviral treatments for infections with further applications to fighting other illnesses with similar mechanisms of action as well as advance our understanding of mucins in the context of airborne transmission.

REFERENCES

(1) Gallagher, T. M.; Buchmeier, M. J. Coronavirus Spike Proteins in Viral Entry and Pathogenesis. *Virology* **2001**, *279* (2), 371–374. https://doi.org/https://doi.org/10.1006/viro.2000.0757.

(2) Lu, G.; Wang, Q.; Gao, G. F. Bat-to-Human: Spike Features Determining 'Host Jump' of Coronaviruses SARS-CoV, MERS-CoV, and Beyond. *Trends Microbiol* **2015**, *23* (8), 468–478. https://doi.org/10.1016/J.TIM.2015.06.003.

(3) Li, F. Structure, Function, and Evolution of Coronavirus Spike Proteins. *Annu Rev Virol* **2016**, *3* (Volume 3, 2016), 237–261. https://doi.org/10.1146/ANNUREV-VIROLOGY-110615-042301/CITE/REFWORKS.

(4) Jackson, C. B.; Farzan, M.; Chen, B.; Choe, H. Mechanisms of SARS-CoV-2 Entry into Cells. *Nat Rev Mol Cell Biol* **2022**, *23* (1), 3–20. https://doi.org/10.1038/S41580-021-00418-X.

(5) Gui, M.; Song, W.; Zhou, H.; Xu, J.; Chen, S.; Xiang, Y.; Wang, X. Cryo-Electron Microscopy Structures of the SARS-CoV Spike Glycoprotein Reveal a Prerequisite Conformational State for Receptor Binding. *Cell Research 2017 27:1* **2016**, *27* (1), 119–129. https://doi.org/10.1038/cr.2016.152.

(6) Zhou, T.; Tsybovsky, Y.; Gorman, J.; Rapp, M.; Cerutti, G.; Chuang, G. Y.; Katsamba, P. S.; Sampson, J. M.; Schön, A.; Bimela, J.; Boyington, J. C.; Nazzari, A.; Olia, A. S.; Shi, W.; Sastry, M.; Stephens, T.; Stuckey, J.; Teng, I. T.; Wang, P.; Wang, S.; Zhang, B.; Friesner, R. A.; Ho, D. D.; Mascola, J. R.; Shapiro, L.; Kwong, P. D. Cryo-EM Structures of SARS-CoV-2 Spike without and with ACE2 Reveal a PH-Dependent Switch to Mediate Endosomal Positioning of Receptor-Binding Domains. *Cell Host Microbe* **2020**, *28* (6), 867-879.e5. https://doi.org/10.1016/j.chom.2020.11.004.

(7) Xiao, T.; Lu, J.; Zhang, J.; Johnson, R. I.; McKay, L. G. A.; Storm, N.; Lavine, C. L.; Peng, H.; Cai, Y.; Rits-Volloch, S.; Lu, S.; Quinlan, B. D.; Farzan, M.; Seaman, M. S.; Griffiths, A.; Chen, B. A Trimeric Human Angiotensin-Converting Enzyme 2 as an Anti-SARS-CoV-2 Agent. *Nature Structural & Molecular Biology 2021 28:2* **2021**, *28* (2), 202–209. https://doi.org/10.1038/s41594-020-00549-3.

(8) McCallum, M.; Walls, A. C.; Sprouse, K. R.; Bowen, J. E.; Rosen, L. E.; Dang, H. V; De Marco, A.; Franko, N.; Tilles, S. W.; Logue, J.; Miranda, M. C.; Ahlrichs, M.; Carter, L.; Snell, G.; Pizzuto, M. S.; Chu, H. Y.; Van Voorhis, W. C.; Corti, D.; Veesler, D. Molecular Basis of Immune Evasion by the Delta and Kappa SARS-CoV-2 Variants. *Science (1979)* **2021**, *374* (6575), 1621–1626. https://doi.org/10.1126/science.abl8506.

(9) McCallum, M.; Czudnochowski, N.; Rosen, L. E.; Zepeda, S. K.; Bowen, J. E.; Walls, A. C.; Hauser, K.; Joshi, A.; Stewart, C.; Dillen, J. R.; Powell, A. E.; Croll, T. I.; Nix, J.; Virgin, H. W.; Corti, D.; Snell, G.; Veesler, D. Structural Basis of SARS-CoV-2 Omicron Immune Evasion and Receptor Engagement. *Science (1979)* **2022**, *375* (6583), 864–868. https://doi.org/10.1126/science.abn8652.

(10) Korber, B.; Fischer, W. M.; Gnanakaran, S.; Yoon, H.; Theiler, J.; Abfalterer, W.; Hengartner, N.; Giorgi, E. E.; Bhattacharya, T.; Foley, B.; Hastie, K. M.; Parker, M. D.; Partridge, D. G.; Evans, C. M.; Freeman, T. M.; de Silva, T. I.; Angyal, A.; Brown, R. L.; Carrilero, L.; Green, L. R.; Groves, D. C.; Johnson, K. J.; Keeley, A. J.; Lindsey, B. B.; Parsons, P. J.; Raza, M.; Rowland-

Jones, S.; Smith, N.; Tucker, R. M.; Wang, D.; Wyles, M. D.; McDanal, C.; Perez, L. G.; Tang, H.; Moon-Walker, A.; Whelan, S. P.; LaBranche, C. C.; Saphire, E. O.; Montefiori, D. C. Tracking Changes in SARS-CoV-2 Spike: Evidence That D614G Increases Infectivity of the COVID-19 Virus. *Cell* **2020**, *182* (4), 812-827.e19. https://doi.org/10.1016/j.cell.2020.06.043.

(11) Hou, Y. J.; Okuda, K.; Edwards, C. E.; Martinez, D. R.; Asakura, T.; Dinnon, K. H.; Kato, T.; Lee, R. E.; Yount, B. L.; Mascenik, T. M.; Chen, G.; Olivier, K. N.; Ghio, A.; Tse, L. V.; Leist, S. R.; Gralinski, L. E.; Schäfer, A.; Dang, H.; Gilmore, R.; Nakano, S.; Sun, L.; Fulcher, M. L.; Livraghi-Butrico, A.; Nicely, N. I.; Cameron, M.; Cameron, C.; Kelvin, D. J.; de Silva, A.; Margolis, D. M.; Markmann, A.; Bartelt, L.; Zumwalt, R.; Martinez, F. J.; Salvatore, S. P.; Borczuk, A.; Tata, P. R.; Sontake, V.; Kimple, A.; Jaspers, I.; O'Neal, W. K.; Randell, S. H.; Boucher, R. C.; Baric, R. S. SARS-CoV-2 Reverse Genetics Reveals a Variable Infection Gradient in the Respiratory Tract. *Cell* **2020**, *182* (2), 429-446.e14. https://doi.org/10.1016/J.CELL.2020.05.042/ATTACHMENT/36CE948B-608F-445B-99E9-C5EB06ACEBAB/MMC1.PDF.

(12) Casalino, L.; Gaieb, Z.; Goldsmith, J. A.; Hjorth, C. K.; Dommer, A. C.; Harbison, A. M.; Fogarty, C. A.; Barros, E. P.; Taylor, B. C.; Mclellan, J. S.; Fadda, E.; Amaro, R. E. Beyond Shielding: The Roles of Glycans in the SARS-CoV-2 Spike Protein. *ACS Cent Sci* **2020**, *6* (10), 1722–1734. https://doi.org/10.1021/ACSCENTSCI.0C01056/SUPPL_FILE/OC0C01056_SI_006.ZIP.

(13) Sztain, T.; Ahn, S. H.; Bogetti, A. T.; Casalino, L.; Goldsmith, J. A.; Seitz, E.; McCool, R. S.; Kearns, F. L.; Acosta-Reyes, F.; Maji, S.; Mashayekhi, G.; McCammon, J. A.; Ourmazd, A.; Frank, J.; McLellan, J. S.; Chong, L. T.; Amaro, R. E. A Glycan Gate Controls Opening of the SARS-CoV-2 Spike Protein. *Nat Chem* **2021**, *13*, 963–968. https://doi.org/10.1038/s41557-021-00758-3.

(14) Cornwell, O.; Radford, S. E.; Ashcroft, A. E.; Ault, J. R. Comparing Hydrogen Deuterium Exchange and Fast Photochemical Oxidation of Proteins: A Structural Characterisation of Wild-Type and ΔN6 B2-Microglobulin. *J Am Soc Mass Spectrom* **2018**, *29* (12), 2413–2426. https://doi.org/10.1007/S13361-018-2067-Y/FIGURES/8.

(15) Tullius, T. D.; Dombroski, B. A. Hydroxyl Radical "Footprinting": High-Resolution Information about DNA-Protein Contacts and Application to Lambda Repressor and Cro Protein. *Proceedings of the National Academy of Sciences* **1986**, *83* (15), 5469–5473. https://doi.org/10.1073/PNAS.83.15.5469.

(16) Maleknia, S. D.; Brenowitz, M.; Chance, M. R. Millisecond Radiolytic Modification of Peptides by Synchrotron X-Rays Identified by Mass Spectrometry. *Anal Chem* **1999**, *71* (18), 3965–3973. https://doi.org/10.1021/AC990500E/ASSET/IMAGES/LARGE/AC990500EF00005.JPEG.

(17) Hambly, D. M.; Gross, M. L. Laser Flash Photolysis of Hydrogen Peroxide to Oxidize Protein Solvent-Accessible Residues on the Microsecond Timescale. *J Am Soc Mass Spectrom* **2005**, *16* (12), 2057–2063. https://doi.org/10.1016/j.jasms.2005.09.008.

(18) Aye, T. T.; Low, T. Y.; Sze, S. K. Nanosecond Laser-Induced Photochemical Oxidation Method for Protein Surface Mapping with Mass Spectrometry. *Anal Chem* **2005**, *77* (18), 5814–5822. https://doi.org/10.1021/AC050353M/ASSET/IMAGES/LARGE/AC050353MF00008.JPEG.

(19) Johnson, D. T.; Punshon-Smith, B.; Espino, J. A.; Gershenson, A.; Jones, L. M. Implementing In-Cell Fast Photochemical Oxidation of Proteins in a Platform Incubator with a Movable XY Stage. *Anal Chem* **2020**, *92* (2), 1691–1696. https://doi.org/10.1021/ACS.ANALCHEM.9B04933/SUPPL_FILE/AC9B04933_SI_001.PDF.

(20) Espino, J. A.; Mali, V. S.; Jones, L. M. In Cell Footprinting Coupled with Mass Spectrometry for the Structural Analysis of Proteins in Live Cells. *Anal. Chem* **2015**, *87*, 41. https://doi.org/10.1021/acs.analchem.5b01888.

(21) Espino, J. A.; King, C. D.; Jones, L. M.; Robinson, R. A. S. In Vivo Fast Photochemical Oxidation of Proteins Using Enhanced Multiplexing Proteomics. *Anal Chem* **2020**, *92* (11), 7596–7603. https://doi.org/10.1021/ACS.ANALCHEM.0C00174.

(22) Xu, G.; Chance, M. R. Hydroxyl Radical-Mediated Modification of Proteins as Probes for Structural Proteomics. *Chem Rev* **2007**, *107* (8), 3514–3543. https://doi.org/10.1021/CR0682047/ASSET/IMAGES/LARGE/CR0682047F00012.JPEG.

(23) Sharp, J. S.; Chea, E. E.; Misra, S. K.; Orlando, R.; Popov, M.; Egan, R. W.; Holman, D.; Weinberger, S. R. Flash Oxidation (FOX) System: A Novel Laser-Free Fast Photochemical Oxidation Protein Footprinting Platform. *Cite This: J. Am. Soc. Mass Spectrom* **2021**, *32*, 1601–1609. https://doi.org/10.1021/jasms.0c00471.

(24) Sharp, J. S.; Misra, S. K.; Persoff, J. J.; Egan, R. W.; Weinberger, S. R. Real Time Normalization of Fast Photochemical Oxidation of Proteins Experiments by Inline Adenine Radical Dosimetry. **2018**. https://doi.org/10.1021/acs.analchem.8b02787.

(25) Chambers, M. C.; MacLean, B.; Burke, R.; Amodei, D.; Ruderman, D. L.; Neumann, S.; Gatto, L.; Fischer, B.; Pratt, B.; Egertson, J.; Hoff, K.; Kessner, D.; Tasman, N.; Shulman, N.; Frewen, B.; Baker, T. A.; Brusniak, M. Y.; Paulse, C.; Creasy, D.; Flashner, L.; Kani, K.; Moulding, C.; Seymour, S. L.; Nuwaysir, L. M.; Lefebvre, B.; Kuhlmann, F.; Roark, J.; Rainer, P.; Detlev, S.; Hemenway, T.; Huhmer, A.; Langridge, J.; Connolly, B.; Chadick, T.; Holly, K.; Eckels, J.; Deutsch, E. W.; Moritz, R. L.; Katz, J. E.; Agus, D. B.; MacCoss, M.; Tabb, D. L.; Mallick, P. A Cross-Platform Toolkit for Mass Spectrometry and Proteomics. *Nat Biotechnol* **2012**, *30* (10), 918–920. https://doi.org/10.1038/NBT.2377.

(26) Rojas Ramírez, C.; Espino, J. A.; Jones, L. M.; Polasky, D. A.; Nesvizhskii, A. I. Efficient Analysis of Proteome-Wide FPOP Data by FragPipe. *Anal Chem* **2023**, *95* (44), 16131–16137. https://doi.org/10.1021/ACS.ANALCHEM.3C02388/ASSET/IMAGES/LARGE/AC3C02388_0004.JPEG.

(27) Rinas, A.; Espino, J. A.; Jones, L. M. An Efficient Quantitation Strategy for Hydroxyl Radical-Mediated Protein Footprinting Using Proteome Discoverer. *Anal Bioanal Chem* **2016**, *408* (11), 3021–3031. https://doi.org/10.1007/S00216-016-9369-3/TABLES/2.

(28) Symmes, B. A.; Stefanski, A. L.; Magin, C. M.; Evans, C. M. Role of Mucins in Lung Homeostasis: Regulated Expression and Biosynthesis in Health and Disease. *Biochem Soc Trans* **2018**, *46* (3), 707–719. https://doi.org/10.1042/BST20170455.

(29) Gan, H. H.; Zinno, J.; Piano, F.; Gunsalus, K. C. Omicron Spike Protein Has a Positive Electrostatic Surface That Promotes ACE2 Recognition and Antibody Escape. *Frontiers in Virology* **2022**, *2*, 894531. https://doi.org/10.3389/FVIRO.2022.894531.

(30) Dommer, A.; Casalino, L.; Kearns, F.; Rosenfeld, M.; Wauer, N.; Ahn, S.-H.; Russo, J.; Oliveira, S.; Morris, C.; Bogetti, A.; Trifan, A.; Brace, A.; Sztain, T.; Clyde, A.; Ma, H.; Chennubhotla, C.; Lee, H.; Turilli, M.; Khalid, S.; Tamayo-Mendoza, T.; Welborn, M.; Christensen, A.; A Smith, D. G.; Qiao, Z.; Krishna Sirumalla, S.; Manby, F.; Anandkumar, A.; Hardy, D.; Phillips, J.; Stern, A.; Romero, J.; Clark, D.; Dorrell, M.; Maiden, T.; Huang, L.; McCalpin, J.; Woods, C.; Gray, A.; Williams, M.; Barker, B.; Rajapaksha, H.; Pitts, R.; Gibbs, T.; Stone, J.; Zuckerman, D.; Mulholland, A.; Miller III, T.; Jha, S.; Ramanathan, A.; Chong, L.; Amaro, R.; Woods, C. #COVIDisAirborne: AI-Enabled Multiscale Computational Microscopy of Delta SARS-CoV-2 in a Respiratory Aerosol. *bioRxiv* **2021**. https://doi.org/10.1101/2021.11.12.468428.

(31) Oswin, H. P.; Haddrell, A. E.; Otero-Fernandez, M.; Mann, J. F. S.; Cogan, T. A.; Hilditch, T. G.; Tian, J.; Hardy, D. A.; Hill, D. J.; Finn, A.; Davidson, A. D.; Reid, J. P. The Dynamics of SARS-CoV-2 Infectivity with Changes in Aerosol Microenvironment. *Proc Natl Acad Sci U S A* **2022**, *119* (27), e2200109119. https://doi.org/10.1073/PNAS.2200109119/SUPPL_FILE/PNAS.2200109119.SAPP.PDF.

(32) D'Imprima, E.; Floris, D.; Joppe, M.; Sánchez, R.; Grininger, M.; Kühlbrandt, W. Protein Denaturation at the Air-Water Interface and How to Prevent It. *Elife* **2019**, *8*. https://doi.org/10.7554/ELIFE.42747.